Journal of Non-Newtonian Fluid Mechanics 309 (2022) 104893

Contents lists available at ScienceDirect

Journal of Non-Newtonian Fluid Mechanics

journal homepage: www.elsevier.com/locate/jnnfm

Effects of fluid–fluid interfacial properties on the dynamics of bounded viscoelastic thin liquid films

Bamikole Adeyemi [a], Prashant Jadhawar [a,*], Lateef Akanji [a], Valeria Barra [b]

[a] School of Engineering, University of Aberdeen, Aberdeen, United Kingdom
[b] California Institute of Technology, Pasadena, CA, United States of America

ARTICLE INFO

Keywords:
Viscoelastic fluids
Interfacial stability
Thin liquid films
Viscoelasticity
Interfacial dynamics

ABSTRACT

The influence of fluid–fluid interfacial properties on the dynamics of viscoelastic thin liquid films bounded above by liquid–liquid interface and below by a horizontal solid plate is studied in this work. The present study allows for integration of both chemical and physical properties of the thin liquid film within the long wave approximation of the evolution equation for viscoelastic thin films. The effects of the contact angle, slippage and exposure time on interfacial film dynamics are verified. We demonstrate the importance of the interfacial tension due to surfactant concentration and the Marangoni number to responses of thin films to prescribed perturbations. The linear stability analysis shows that the rupture time is dependent on the initial tension, Marangoni number, slippage and contact angle, whereas the cut off wavenumber is only affected by the contact angle. Results of the numerical simulations of the nonlinear regime show that the film dynamics is faster with slippage and exposure time. We confirm that viscoelasticity increases the number of droplets formed after the film rupture. However, the linear relationship between interfacial tension and surfactant concentration fails to describe the thin film dynamics when the Weissenberg number exceeds the Reynolds number.

1. Introduction

Stability of thin films is an important aspect of surface and interface interactions, and it has received wide attention in the literature [1–7]. Almost all petroleum, chemical and biomedical engineering processes that involve applications of liquid mixtures consider the forces at play on interfaces especially when the interfacial pressure could lead to film rupturing [8]. Theoretically, there exist at least two mathematical interfaces (fluid–solid and fluid–fluid) when liquid films spread on solid surfaces [9,10]. These interfaces can overlap depending on the wettability of the rock surface. The effect of disjoining pressure is said to be significant on both boundaries. The fluid–fluid interface is therefore constantly under disjoining pressure which tends to separate it from the fluid–solid interface [11].

The nonlinear evolution of free films (not necessarily of viscoelastic type) with the presence of surfactants has also received considerable attention in the literature [2,12–14] since the linear theory on free film bounded by two free surfaces presented by Ruckenstein and Jain [15]. Wit et al. [13] extended the work of Maldarelli et al. [12] by developing the nonlinear evolution equation for free films with insoluble surfactants. In their work, the authors showed that the region of film stability depends on the van der Waals attraction and interfacial tension. It was shown that increasing the Marangoni number decreases the growth rate of the perturbation, and increases thus the time of rupture of the film. The authors concluded that surfactant monolayer has a stabilizing effect on the growth of the instability. Moreover, the flow dynamics in a rupture case indicates that the surfactants will flow away from the depressions of the thickness of the film to concentrate at its elevations. Kovalchuk and Vollhardt [16] presented the criteria of instability for the surfactant transfer through a liquid interface. The authors indicated that the instability criteria are dependent on interfacial structure (planar or spherical), surface area, thickness of the liquid layers and the relationship between rates of diffusion and adsorption. Agble and Mendes-Tatsis [17] studied the instability of various binary liquid–liquid interfaces in the presence of surfactant transferring.

The interfacial tension gradient due to surfactant concentration disturbance induces Marangoni instability and has been widely reported in the literature since Pearson [18] and Sternling and Scriven [19]. Marangoni instability in liquid/liquid systems occurs with the presence of bulk concentration gradient normal to the interface. Marangoni instability is a subject of interest since the interface instability significantly promotes interfacial mass transfer [20]. Slavtchev et al.

* Corresponding author.
E-mail address: Prashant.Jadhawar@abdn.ac.uk (P. Jadhawar).

https://doi.org/10.1016/j.jnnfm.2022.104893
Received 3 February 2022; Received in revised form 9 June 2022; Accepted 3 August 2022
Available online 6 August 2022

Nomenclature

β	Elasticity number
δh_0	Amplitude of the Fourier mode
$\dot{\gamma}$	Strain rate tensor
κ	Local curvature
λ_1	Relaxation time
λ_2	Retardation time
$\mathbf{n}$	Outward unit normal
μ	Dynamic viscosity
ν	Kinematic viscosity
ω	Growth rate
ρ	Density
Σ	Dimensionless interfacial tension
σ	Interfacial tension
σ_0	Dimensionless interfacial tension for the constant part of the interfacial tension
θ	Contact angle
φ	Tangential stress
$\vec{\tau}$	Stress tensor
b	Slip coefficient
C	Dimensionless surfactant concentration
C_0	Equilibrium surfactant concentration
h_0	Mean thickness
I	Identity matrix
k	Wavenumber
k_c	Cut off wavenumber
k_m	Wavenumber of maximum growth
M	Marangoni number
P	Dimensionless capillary pressure
p	Capillary pressure
Re	Reynolds number
t	Exposure time
u	Velocity component in longitudinal direction
v	Velocity component in transverse direction
W	Dimensionless van der Waals induced by disjoining pressure
w	Normal stress
Wi	Weissenberg number
x	Longitudinal direction
x_{CO}	Dimensionless surfactant coverage
y	Transverse direction

[21] studied the onset of Marangoni instability in partially miscible liquid–liquid systems in the presence of surface-active solutes. Their study indicated that the stability conditions depend mainly on physical parameters of the system, such as the solute diffusivity ratio and the kinematic viscosity ratio. Slavtchev et al. [22] studied the influence of low frequency vibration on Marangoni instability in a layer of binary mixture. Their results indicated that the vibration destabilizes the layer and the instability takes place even for zero Marangoni number. The above approaches only discuss Marangoni instability and rarely consider the important effects of viscoelasticity which is a significant factor in any liquid flow near the interface, and in the stability of the thin films separating emulsion drops or foam bubbles [23]. Surfactant-covered bodies such as those exposed to a fluid–fluid interface possess own elasticity and viscosity relating to the non-equilibrium values of the interfacial tension and are described using viscoelasticity.

Extending the lubrication model for thin viscoelastic films of Jeffreys types developed in [24], a computational investigation of thin viscoelastic films and drops on a solid substrates, subjected to the van der Waals interaction force in two spatial dimensions was presented initially in the absence of gravity in [1], and subsequently including the competing effects of the gravitational force in [25]. in [1], the authors verified that, in absence of other external driving mechanisms such as gravity, the van der Waals interaction force drives the instabilities of liquid interface and causes the film to break up, forming holes bounded by retracting rims. Furthermore, the investigation presented in [1] shows that the dewetting of thin viscoelastic films in the nonlinear regime reveals novel complex morphologies that depend on viscoelasticity. However, in the existing literature, the assumption of constant surface tension idealized the model by simplifying the fluid–fluid interfacial boundary description. Consequently, in some of the existing studies, it is difficult to ascertain the importance of surface tension on the fluid–fluid interfaces, in addition to the fluid rheological properties, while evaluating the dynamics of viscoelastic thin films.

The stability of a thin film of Walters-type B" viscoelastic fluid flowing down a heated inclined plane was investigated by Fu et al. [26]. The authors studied the effects of the Marangoni number, viscoelastic parameter and Biot number. In that study, the authors found that the stability of the thin films under the prescribed condition is weakened by viscoelasticity and thermocapillarity. In addition, the authors demonstrated that increase in Marangoni number leads to expansion of the region of instability of the films. The authors, however, reported a reduction in the accuracy of their model with increase of the Marangoni number. Sarma and Mondal [27] investigated the Marangoni instability in a thin polymeric liquid film heated from the free surface. The authors established that, for heating a thin polymeric film from the free surface, the solutocapillary force often can destabilize a system which otherwise remains stable under the action of thermocapillarity.

In this work, the viscoelastic thin film evolution base model [1,24] is modified to accommodate gradients of interfacial tension that may occur in fluids with and without surfactants [13]. Integrating interfacial tension gradients allows us to evaluate the influence of the Marangoni number, initial interfacial tension, and surfactant concentration on the dynamics of viscoelastic thin films. We begin the modification by representing the surface tension term in the expression for stress balance at the interface with a dimensionless linear relationship. Various physical properties of the thin liquid film can thus be defined within this expression. Generally, the interest to include thin liquid film properties emanates from the application of thin film theory to substance mixing which requires surfactant effects. Subsequently, the expression for surface tension is integrated into the asymptotic expansion of the stress balance as described by [24]. Scaling the surface tension term reveals its influence on the capillary term of the final evolution equation and therefore allows us to verify the effects of individual physical properties on interfacial dynamics of thin liquid films. We verify the effects of the viscoelastic characteristic times, i.e. relaxation and retardation times, slip coefficient and the exposure time. Subsequently, the influence of all physical parameters in the present model are investigated. Finally, the relevance of the relationship between interfacial tension and surfactant concentration, whether linear or nonlinear, on the dynamics of thin liquid films is studied.

The rest of the paper is organized as follows: The formulation of the nonlinear evolution equation for the problem is discussed in Section 2. In Section 3, we perform the linear stability analysis (LSA) to confirm and demonstrate the roles of the relevant parameters on the dynamics of the evolved free films while the numerical simulations of the dynamic behaviour of the system under different conditions are presented in Section 4. The analysis of the shape in the dewetted region is discussed in Section 5 and the conclusion drawn from the results of this study is presented in Section 6. Derivation of the full long wave approximation described in this study is presented in the Appendix.

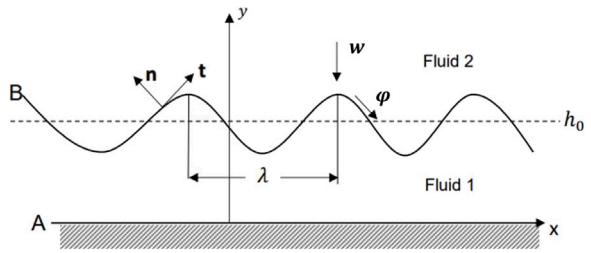

Fig. 1. Geometry of a thin liquid film bounded below by a horizontal plate, *A* and above by the fluid–fluid interface, *B*. The height, h_0, represents the mean thickness of the viscoelastic thin liquid film. The prescribed forcing at the interface is composed of the normal and tangential stresses, w and φ respectively.

2. Model development

The lubrication approximation is applied to a system consisting of a viscoelastic thin liquid film bounded by two interfaces that can be described mathematically. The system is bounded above and below by liquid–liquid and liquid–solid interfaces, respectively. The interfacial properties are assumed to respond to any changes caused by addition of surfactant in the thin liquid film. Fig. 1 shows the schematic of the thin liquid film geometry where the longitudinal direction is denoted by x, the transverse direction by y, and the respective velocity components by u and v. The liquid film is assumed to be thin enough that van der Waals forces are effective and thick enough that a continuum theory of the liquid is applicable. The free surface of the film, defined by $y = h(x,t)$, is subject to an external normal stress, w, and a tangential stress, φ.

The general Navier–Stokes and the continuity equations for incompressible fluids are of the form

$$\rho\left(\frac{\partial \mathbf{u}}{\partial t} + \mathbf{u}\cdot\nabla\mathbf{u}\right) = -\nabla(p+w) + \nabla\cdot\vec{\tau}, \tag{1}$$

$$\nabla\cdot\mathbf{u} = 0, \tag{2}$$

where $\nabla = (\partial_x, \partial_y)$, $\mathbf{u} = (u,v)$ is the velocity and p is the capillary pressure, w is the normal stress which corresponds to the van der Waals induced disjoining pressure and $\vec{\tau}$ is the stress tensor.

To derive the equations that will apply to continuous liquid films on a horizontal plate, which spread and displace the surrounding fluid, a condition of no penetration and a Navier type model that relates slip to shear stress are assumed, i.e.,

$$v = 0, \quad u = \frac{b}{\eta}\tau_{21}, \qquad \text{at } y = 0, \tag{3}$$

where the slip coefficient, b, is zero when a no-slip boundary condition is considered.

At $y = h(x,t)$, the kinematic boundary condition (in the absence of interfacial mass transfer), which balances the normal component of the liquid velocity at the interface with the speed of the interface, is given as

$$v = \frac{\partial h}{\partial t} + u\frac{\partial h}{\partial x}. \tag{4}$$

The stress balance at the interface is given by

$$(\tau - (p+w)I)\cdot\mathbf{n} = \sigma\kappa\mathbf{n}, \tag{5}$$

where $\mathbf{n}$ is the outward unit normal, I is the identity matrix with same dimensionality of the problem. $\kappa = -\nabla\cdot\mathbf{n}$ and σ are the local curvature and the interfacial tension respectively.

The viscoelastic stresses are modelled by applying the linear Jeffreys model which is expressed as [28]

$$\tau + \lambda_1\frac{\partial\tau}{\partial t} = \mu\left(\dot{\gamma} + \lambda_2\frac{\partial\dot{\gamma}}{\partial t}\right), \tag{6}$$

where $\dot{\gamma}$ is the strain rate tensor, e.g. $\dot{\gamma}_{12} = \partial_x u + \partial_y v$ (other components of $\dot{\gamma}$ are similarly expressed in terms of derivatives of $\mathbf{u}$). In this model, the response to the deformation of a viscoelastic liquid is characterized by two-time constants, λ_1 and λ_2, called the relaxation time and the retardation time, respectively.

The long-wave approximation theory requires that appropriate scaling, which relates the thin film height to its lateral extension, is applied. Introducing the scale h_0 towards the film height direction and L for the lateral direction, the distortion can be of long scale if

$$\epsilon = \frac{h_0}{L} \ll 1. \tag{7}$$

We can further define the dimensionless capillary pressure, P and the dimensionless van der Waals induced disjoining pressure, W, as

$$(P, W) = \frac{1}{p_0}(p, w). \tag{8}$$

The dimensionless interfacial tension, Σ, resulting from the changes caused by surfactant addition to the system is

$$\Sigma = \frac{\epsilon^2\sigma}{\mu u_0}. \tag{9}$$

The leading-order terms of the normal and tangential components of the stress balance at the free surface respectively (shown in Appendix) are

$$P = -\Sigma\frac{\partial^2 h}{\partial x^2} - W(h), \qquad \text{at } y = h(x,t), \tag{10}$$

$$\frac{\partial h}{\partial x}\tau_{21} = 0. \tag{11}$$

Contrary to earlier simplifications by Rauscher et al. [24], it is clear from Eq. (10) that the capillary term of the pressure field is influenced by dimensionless interfacial tension at the fluid–fluid interface. It is therefore essential to retain interfacial tension effects at the leading order. Hence, the effects of fluid properties can be studied even if there is no interionic reactions at the fluid–solid interface.

The system under consideration consists of an incompressible thin liquid film of initial, unperturbed thickness h_0, density ρ, kinematic viscosity ν, and dynamic viscosity μ. The film is expected to be of finite extent with its length, L, greatly exceeding its thickness, h_0. The fluid–fluid interface possesses properties such as interfacial tension and surface coverage. Consequently, if the surfactants are free to flow along the interface, the interfacial tension gradient will develop depending on surfactant concentration at the interface [19]. Other dimensionless variables can be introduced using the following scales

$$\begin{aligned} &\text{length} = h_0, \quad \text{time} = \frac{h_0^2}{\nu}, \\ &\text{velocity} = \frac{\nu}{h_0} \quad \text{and} \quad \text{pressure} = \frac{\rho\nu^2}{h_0^2}. \end{aligned} \tag{12}$$

To proceed from the findings from previous studies [1–3,29], we consider the spatial variation of surfactant concentration, C, along the interfaces which gives rise to interfacial shear stress. Interfacial tension is assumed to decrease linearly with surfactant concentration [4], so that

$$\Sigma = \Sigma_0 - MC, \tag{13}$$

where

$$\Sigma_0 = \frac{\sigma_0 h_0}{\rho\nu^2} \tag{14}$$

is the dimensionless interfacial tension for the constant part of the interfacial tension, σ_0, at the equilibrium concentration, C_0, and M is the solution version of the Marangoni number, proportional to

$$M = -C_0\left(\frac{h_0}{\rho\nu^2}\right)\left(\frac{\partial\sigma}{\partial C}\right), \tag{15}$$

where we remind the reader that σ is the dimensional interfacial tension, and the dimensionless surfactant concentration is expressed as $C = C/C_0$. Hence,

$$p = -\left(\Sigma_0 - M_s C\right)\left(\frac{\partial^2 h}{\partial x^2}\right) - W(h). \tag{16}$$

The final dimensionless form of the nonlinear evolution equation for bounded viscoelastic thin films is

$$\left(1+\lambda_2\frac{\partial}{\partial t}\right)\frac{\partial h}{\partial t}+\frac{\partial}{\partial x}\left\{(\lambda_2-\lambda_1)\left(\frac{h^2}{2}Q-hR\right)\frac{\partial h}{\partial t}+\left[\left(1+\lambda_1\frac{\partial}{\partial t}\right)\frac{h^3}{3}+\left(1+\lambda_2\frac{\partial}{\partial t}\right)bh^2\right]\frac{\partial}{\partial x}\left(\Sigma\frac{\partial^2 h}{\partial x^2}-W(h)\right)\right\}=0, \tag{17}$$

where, for compactness, Q and R have been used such that

$$\left(1+\lambda_2\frac{\partial}{\partial t}\right)Q=-\frac{\partial}{\partial x}\left(\frac{\partial p}{\partial x}\right), \tag{18}$$

$$\left(1+\lambda_2\frac{\partial}{\partial t}\right)R=-h\frac{\partial}{\partial x}\left(\frac{\partial p}{\partial x}\right). \tag{19}$$

The equilibrium contact angle, θ_e, which indicates the wetting condition of the solid substrate is included directly into a disjoining pressure, $W(h)$, in the expression which has been applied to thin liquid films of this nature [1,30–32] as follows

$$W(h)=\frac{\sigma\left(1-cos\theta_e\right)}{Nh_*}\left[\left(\frac{h_*}{h}\right)^{n_1}-\left(\frac{h_*}{h}\right)^{n_2}\right], \tag{20}$$

with

$$N=\frac{\left(n_1-n_2\right)}{\left[\left(n_1-1\right)\left(n_2-1\right)\right]}, \tag{21}$$

where n_1 and n_2 are constants such that $n_1 > n_2 > 1$. Several values of (n_1, n_2) have been experimented in the literature and $(3, 2)$ which have been widely used [1,30–32] are chosen for this work. σ and h_* are the interfacial tension and the equilibrium thickness introduced by the van der Waals potential respectively.

The physical implication of the Marangoni number on residual oil mobilization is captured in the ability of thin liquid films to withstand snap-off. Snap-off occurs when a mobilized oil droplet breaks up into daughter droplets due to the compression it encounters while being forced through the narrow ducts (pore throats) connecting two pore spaces [33]. Integration of the Marangoni effects into the original evolution equation for thin viscoelastic films allows us to reliably evaluate the contributions of solutocapillarity on the interfacial dynamics of the prescribed films.

3. Linear stability analysis

The response of the developed thin liquid films to prescribed disturbances is studied by performing a linear stability analysis (LSA). A flat film of initial thickness, h_0, containing a unitary surfactant concentration at zero velocity is considered. Hence, we seek a solution of the kind

$$h(x,t)=h_0+\delta h_0 exp(\omega t+ikx). \tag{22}$$

where δh_0 is the amplitude of the Fourier mode, ω is the growth rate and k is the wavenumber. The dispersion relation and corresponding characteristic for the growth rate is obtained:

$$\lambda_2\omega^2+\left[1+(\Sigma k^4-k^2W(h_0))\left(\lambda_1\frac{h_0^3}{3}+\lambda_2 bh_0^2\right)\right]\omega+(\Sigma k^4-k^2W(h_0))\left(\frac{h_0^3}{3}+bh_0^2\right)=0, \tag{23}$$

and the cut off wavenumber k_c for which $\omega = 0$ is implicitly defined by the following relationship

$$k_c^2=\frac{W(h_0)}{\Sigma}. \tag{24}$$

The relationship that describes the cut off wavenumber in Eq. (24), agrees with the linear theory results of viscous thin liquid films previously reported in [13,15]. The wavenumber of maximum growth, $k_m = k_c/\sqrt{2}$ does not depend on the characteristic viscoelastic properties, λ_1 and λ_2, or on the slippage but on the critical contact angle, included in the disjoining pressure term $W(h)$, and the dimensionless interfacial tension, Σ, as dictated by the surfactant concentration. This implies that the domain of stable wavenumbers of free films is controlled by the critical contact angle and the dimensionless interfacial tension. We only analyse the roots of the quadratic Eq. (23) for $k_c^2 = W(h_0)/\Sigma$ since our interest is to have a qualitative understanding of how the physical parameters of the problem affect the domain of unstable wave numbers and the rupture time. We obtain two roots, one of which has varying sign and another root which is strictly negative for $k_c^2 < W(h_0)/\Sigma$. The positive growth rate denotes that the film is mostly unstable. The domain of unstable wave can shrink by reducing the surfactant concentration.

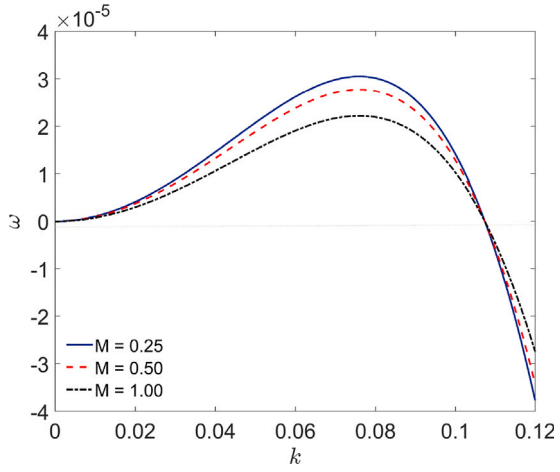

Fig. 2. Growth rate of viscoelastic thin liquid films plotted for surfactant concentration, $C = 1$, slip coefficient, $b = 0$, initial interfacial tension, $\Sigma_0 = 3$ and contact angle, $\theta = 45°$ showing the effects of increasing values of: Marangoni number, $M = 0.25$ (blue solid line), 0.5 (red dashed lines), 1 (black dashed lines). Increasing M leads to a decrease in maximum growth rate and hence to a increase of the rupture time.

We can draw several conclusions by considering the influence of the Marangoni number, the contact angle, the slip coefficient, and the dimensionless interfacial tension, on the maximum growth rate and the cut off wavenumber. We choose parameter values in Table 1 which are consistent with the orders of magnitude of the development according to the procedure established by Wit et al. [13]. The properties of the thin films encountered in oil–brine–rock system are within the chosen range of values [34–37].

Fig. 2 shows a decrease in the maximum growth when the value of M (dimensionless) is doubled from 0.25 to 0.5 and eventually to 1. This observation can be explained by the phenomenon of the Marangoni effect. Because of the depletion of surfactant at the centre of the thin film interface, a diffusion flux is generated in the opposite direction of the drainage, increasing the rigidity of the interface and slowing fluid drainage. Increasing M does not affect the cut off wavenumber which means that the domain of unstable wave number of viscoelastic thin liquid films is the same irrespective of surfactant concentration. The rupture time of the films will increase in response to a decrease in the maximum growth rate. In fact, these two quantities are inversely proportional to each other. The stability of the films, therefore, can be enhanced by an increase in the initial concentration of surfactants in the film or the rate of interfacial tension gradient, $\partial\sigma/\partial C$, to increase the Marangoni number.

The response of the films to an increase in the constant part of the dimensionless interfacial tension, Σ_0, takes an opposite trend compared to the effect of variation of M, on the films. Increasing the dimensionless tension from 3 to 4 leads to increased maximum growth rate, as

Table 1
Constant parameters for both the Linear Stability Analysis (LSA) and the numerical simulations [13].

Parameter	Symbol	Best estimates
Equilibrium interfacial tension	σ_0	1–30 [dyn cm^{-1}]
Equilibrium contact angle	θ	15–45°
kinematic viscosity	ν_p	10^{-2} [cm^2 s^{-1}]
Film viscosity	μ	10^{-2} [g cm^{-2}]
Density of thin film	ρ	1.0 [g cm^{-1}]
Equilibrium thin film thickness	h_0	10^{-6}–10^{-5} [cm]
Dimensionless interfacial tension	$\Sigma_0 = \sigma_0 h_0/\rho\nu_s^2$	10^{-2}–4
Equilibrium surfactant concentration	C_0	10^{-12}–10^{-10} [mol cm^{-2}]
Dimensionless Marangoni number	$M = -C_0\left(\frac{h_0}{\rho\nu^2}\right)\left(\frac{\partial\sigma}{\partial C}\right)$	10^{-5}–1

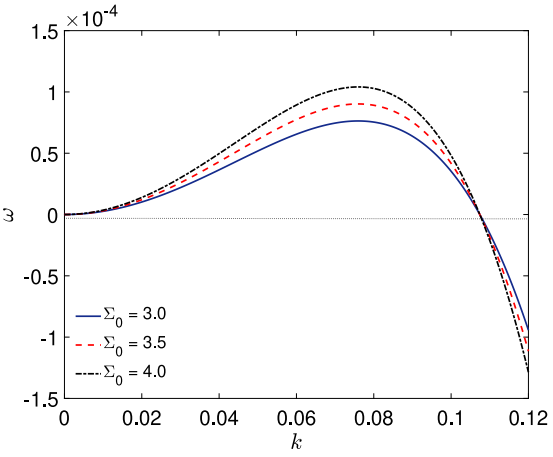

Fig. 3. Growth rate of viscoelastic thin liquid films plotted for surfactant concentration, $C = 1$, slip coefficient, $b = 0$, Marangoni number, $M = 0.25$ and contact angle, $\theta = 45°$ showing the effects of increasing values of initial interfacial tension, $\Sigma_0 = 3$ (blue solid line), 3.5 (red dashed lines), 4 (black dotted lines). Increasing the constant part of the dimensionless interfacial tension Σ_0 leads to an increase in maximum growth rate and hence to a decrease of the rupture time.

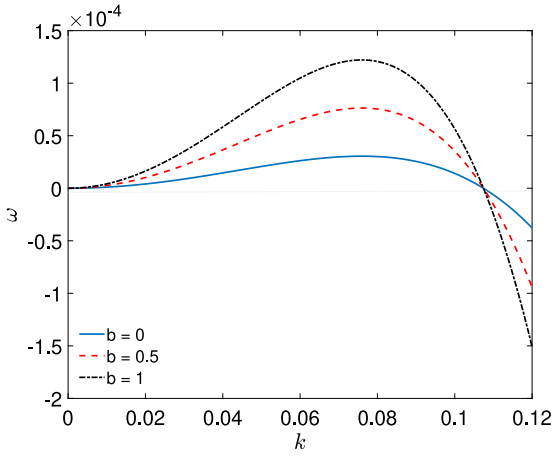

Fig. 4. Growth rate of viscoelastic thin liquid films plotted for surfactant concentration, $C = 1$, Contact angle, $\theta = 45°$, Marangoni number, $M = 0.25$ and dimensionless interfacial tension, $\Sigma_0 = 3$ showing the effects of increasing values of slip coefficient, $b = 0$ (blue solid line), 0.5 (red dashed lines), 1 (black dotted lines). Increasing b leads to an increase in maximum growth rate and hence to a decrease of the rupture time.

shown in Fig. 3. However, as mentioned above, the cut off wavenumber, is not affected by variation in the constant part of the dimensionless interfacial tension. Consequently, the domain of stable/unstable modes remains unchanged with varying interfacial tension, but the rupture time decreases due to the upward trend of the maximum growth rate. This observation shows that films with higher interfacial tension will experience greater instabilities when a prescribed disturbance is applied.

There is decrease in the rupture time when the films respond to increased slip coefficient. In fact, as found in [1], the maximum growth rate increases with increasing slip coefficient, as also shown in Fig. 4, though the domain of unstable mode is constant. Contrarily, variations in contact angle results in corresponding changes in maximum growth rate and cut off wavenumber, as shown in Fig. 5. Increasing the contact angle shortens the domain of instability and decreases the rupture time. This latter behaviour is similar to the observed response of the films to increased slip coefficient. The dynamics of the film rupture which strongly depends on the nonlinear interactions of prescribed disturbances can only be determined by numerical solutions to the viscoelastic thin film equation that we are going to present in the next section.

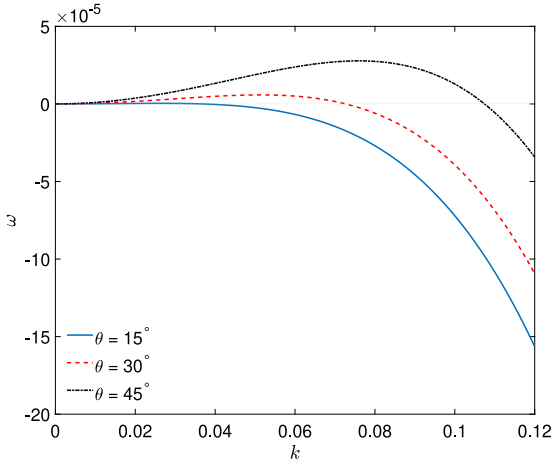

Fig. 5. Growth rate of viscoelastic thin liquid films plotted for surfactant concentration, $C = 1$, slip coefficient, $b = 0$, Marangoni number, $M = 0.25$ and dimensionless interfacial tension, $\Sigma_0 = 3$ showing the effects of increasing values of Contact angle, $\theta = 15°$ (blue solid line), 30° (red dashed lines), 45° (black dotted lines). Increasing θ leads to an increase in the cut off wavenumber and maximum growth rate and hence to a decrease of the wavelength of maximum instability, and a decrease in the rupture time.

4. Numerical implementation

The results of the numerical simulations of the film dynamics are presented in this section. All numerical results regarding the nonlinear dynamics are obtained by using the software by Barra et al. publicly available at Barra [38] and extending it to include interfacial tension variations. We solve the set of Eqs. (1) by discretizing the dimensionless Eq. (17) using finite difference method and Newton's method according to Kondic [39] and Barra et al. [1]. The time derivatives

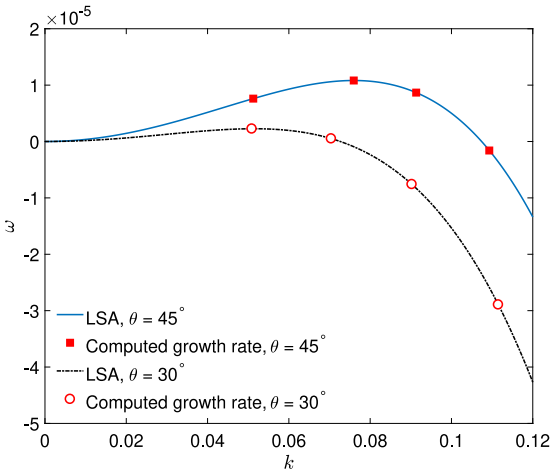

Fig. 6. The comparison of the computed growth rate against the LSA viscoelastic thin liquid films plotted for surfactant concentration, $C = 1$, slip coefficient, $b = 0$, Marangoni number, $M = 0.25$ and dimensionless interfacial tension, $\Sigma_0 = 1$ for contact angles, $\theta = 30°$ and $\theta = 45°$.

are isolated from the spatial ones, so that an iterative scheme can be applied to find the approximation to the solution at the new time step. The time derivatives are then integrated according to the Crank–Nicolson scheme. An initial flat fluid interface of thickness, $h_0 = 1$ is perturbed with $k = k_m$ and $\delta = 0.01$. The spatial domain [0, L] is discretized so that it is divided in uniform intervals, with spatial mesh size $\Delta x = 0.005$. L is chosen to have the domain of maximum growth rate for instability with $L = 2\pi/k_m$. The numerical discretization of the governing PDEs were performed using the procedure outlined in [1]. At the endpoints of the domain, the $\partial h/\partial x = \partial^3 h/\partial x^3 = 0$ boundary conditions are imposed. The condition $h_x = 0$ gives the value of h at the two ghost points x_0 and x_{N+1} outside the physical domain, i.e. $h_0 = h_1$ and $h_{N+1} = h_N$; the condition $\partial^3 h/\partial x^3 = 0$ specifies the two ghost points x_{-1} and x_{N+2}, i.e. $h_{-1} = h_2$ and $h_{N+2} = h_{N-1}$.

The linear equations obtained from discretization and linearization are solved by a direct solver following the numerical procedure outlined in [1]. The values of the Marangoni numbers used for the numerical simulations are similar to the ones used for the linear stability analysis. A normalized surfactant concentration is assumed throughout the simulations and a 45° contact angle is used for clarity of distinctions among the results since the effects of other values of contact angles studied in the LSA show similar trend for the influence of other tested parameters. The numerical results are validated using the methods explained by Barra et al. [1]. The computed growth rates are compared with the theoretical values given by the LSA as shown in Fig. 6. The validation was completed across two values of contact angle, $\theta = 30°$ and $\theta = 45°$.

The responses of the films to prescribed perturbations are experimented for viscoelastic thin films at three different time scales. The time scales are referred to as early, middle and late regimes to follow the dynamics of the films to rupture. The early time corresponds to the initial stage/phase of film deformation when the impact of the perturbation is just noticeable, the middle regime indicates the morphology of the films after later than the early stage and before film rupturing. The late regime shows the time when the film is just about to rupture or has ruptured. These time scales are chosen based on the response of the film with the lowest parameter values.

There is no significant difference in the responses of the films based on the increase of retardation time, $\lambda_2 > 0$, throughout the three regimes. Hence, one figure each is used to represent the film dynamics whether $\lambda_2 = 0$ or $\lambda_2 = 0.01$ to avoid unnecessary repetition of figures. Fig. 7 shows the evolution and growth of the films with different values of the Marangoni number, during the early regime when $t = 3.45 \times 10^5$.

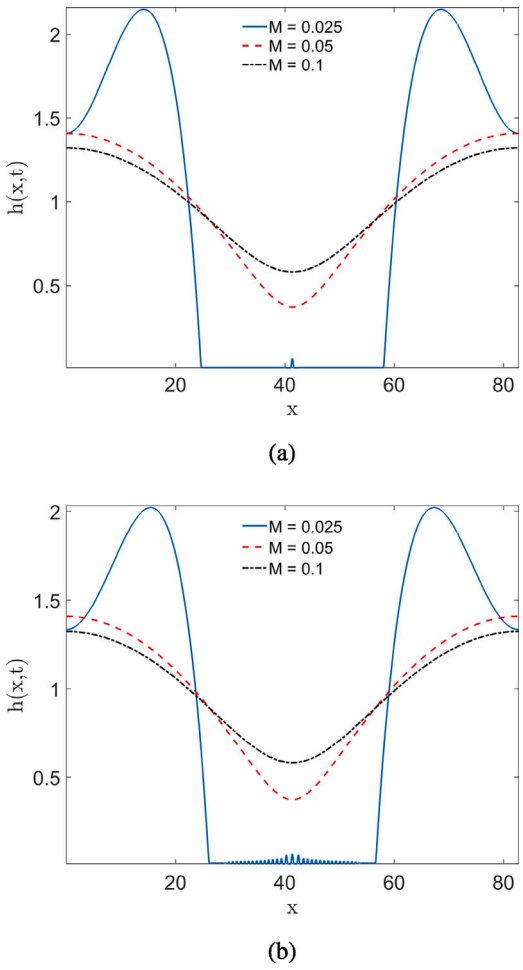

Fig. 7. Evolution of three thin films for $b = 0$, $\lambda_2 = 0.01$, $M = 0.025$ (blue solid lines), 0.05 (red dashed lines), 0.1(black dotted lines) at early time regime, $t = 3.45 \times 10^5$, when (a) $\lambda_1 = 4$ and (b) $\lambda_1 = 10$.

Smaller values of M are chosen for the nonlinear analysis to show the significant impact of M on the film morphology compared to the larger value of M chosen for the linear stability analysis for magnification purpose to show clearly the impact of contact angle. The influence of the Marangoni number is evident in the film behaviour and responses to perturbations. The film with $M = 0.025$ is fully developed and separated into rims in the early regime, while the films with $M = 0.05$ and $M = 0.1$ are respectively still in the developing stages but the film with $M = 0.05$ is ahead of the other, as shown in Fig. 7(a). It is noted that the growth rate of the films is reduced by an increased Marangoni number.

The influence of an increased relaxation time, λ_1, is investigated on the responses of the films according to the values of Marangoni numbers. Fig. 7(b) shows the film behaviour when $\lambda_1 = 10$ and $\lambda_2 = 0.01$ at $t = 3.45 \times 10^5$. Increasing the relaxation time shows observable effects on the film with maximum growth rate or the fully developed film with $M = 0.025$. There is no observable differences in the film height and the film morphology compared with the film height resulted from $\lambda_1 = 4$ at the same time regimes other than the formation of secondary droplets which are more in number when $\lambda_1 = 10$.

During the middle time regime when $t = 3.56 \times 10^5$, as shown in Fig. 8, the two films with 0.025 and 0.05 Marangoni number, respectively, had fully developed with higher thicknesses compared to the films state in the earlier time regime. There are, however, multiple droplets formed due to an increment in the relaxation time from $\lambda_1 = 4$ (see Fig. 8(a)) to $\lambda_1 = 10$, as shown in Fig. 8(b). While the number of

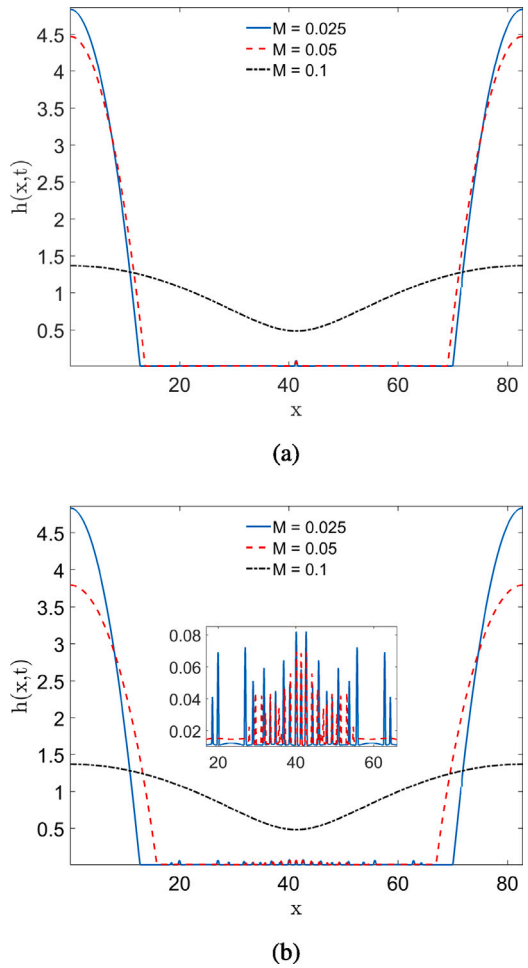

Fig. 8. Evolution of three thin films for $b = 0$, $\lambda_2 = 0.01$, $M = 0.025$ (blue solid lines), 0.05 (red dashed lines), 0.1 (black dotted lines) at middle time regime, $t = 3.56 \times 10^5$, when (a) $\lambda_1 = 4$ and (b) $\lambda_1 = 10$. The insert is a closed in on the secondary droplets caused by the increase in characteristic relaxation time.

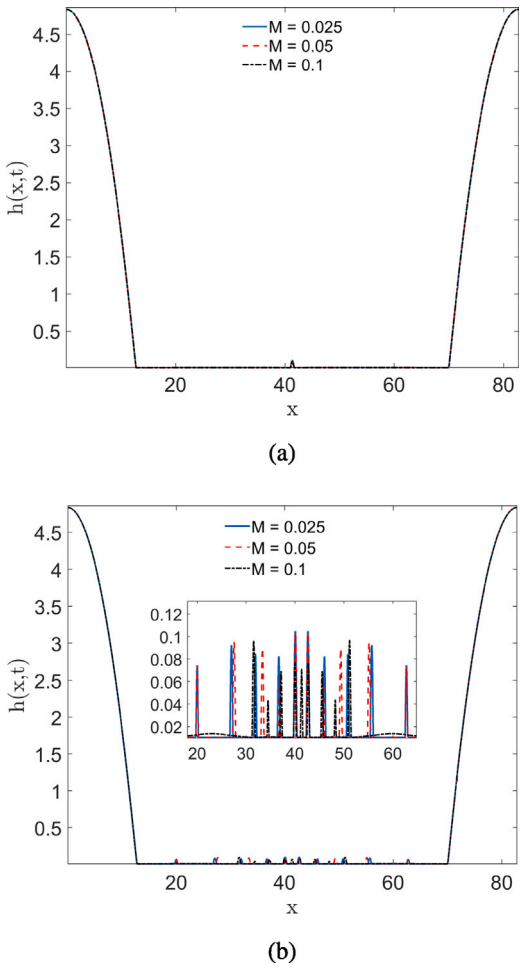

Fig. 9. Evolution of three thin films for $b = 0$, $\lambda_2 = 0.01$, $M = 0.025$ (blue solid lines), 0.05 (red dashed lines), 0.1(black dotted lines) at late time regime, $t = 4.0 \times 10^5$, when (a) $\lambda_1 = 4$ and (b) $\lambda_1 = 10$. The insert is a closed in on the secondary droplets caused by the increase in the characteristic relaxation time.

droplets is higher for $M = 0.025$ and $M = 0.05$ at $\lambda_1 = 10$, the growth of the height of the rims for $M = 0.05$ is higher at $\lambda_1 = 4$.

Fig. 9(a) shows that the films have fully formed and the rim separated at the late regime when $t = 4.0 \times 10^5$. The film responses are the same irrespective of the amount of Marangoni numbers. While the films with $\lambda_1 = 4$ have only one droplet, the films with $\lambda_1 = 10$ ruptured into multiple secondary droplets in Fig. 9(b). These observations point to the importance of the relaxation time in the film evolution process, which have also been reported in [1]. In addition to this, the number of secondary droplets and the speed at which they are formed when $\lambda_1 = 10$ are dependent on Marangoni number. Number of droplets decreases from 13 in the absence of Marangoni effect [1], 10 when $M = 0.025$ and 0.05 to 9 at $M = 0.1$. Besides, increasing the Marangoni number leads to delays in the formation of secondary droplets.

To investigate the effects of the slip coefficient on the dynamics of the evolved thin liquid films, previous Figs. 7–9 are repeated, but with a fixed $b = 1$. The results show that the dynamics with slip coefficient is faster. Similar results were also reported by Barra et al. [1] when non-zero slip coefficients were studied. It can be seen in Figs. 10(a) and 10(b) that the perturbation have grown significantly and the film with $M = 0.025$ has already retracted at time $t = 8.16 \times 10^4$. Subsequently at times $t = 8.2 \times 10^4$ (Fig. 11) and $t = 8.5 \times 10^4$ (Fig. 12) respectively, the films with $M = 0.025$ and $M = 0.05$ have already fully developed. It can also be seen that there are no formation of secondary droplets at $b = 1$.

The influence of the slip boundary condition is tested to study the dynamics of the films at the three-time regimes. Fig. 13 shows the comparisons of the evolved films with $M = 0.025$ when the slip coefficient, $b = 0$ and $b = 1$, at three different time regimes in Figs 13(a)–13(c). It is noted that all the multiple secondary droplets introduced by larger value of relaxation time disappeared when a higher slip coefficient is considered. There are no observable effects of time scales (see Fig. 13) on the dynamics of the films with $b = 1$. The films that are already fully developed at the early time regime when $t = 3.45 \times 10^5$ (Fig. 13(a)) remain unchanged at $t = 3.56 \times 10^5$ (Fig. 13(b)) and $t = 4.0 \times 10^5$ (Fig. 13(c)). In comparison with the findings in [1] for no-slip boundary conditions, the presence of Marangoni number decreases the rupture time and leads to increasing number of secondary droplets formed (Fig. 13(a)).

The focus of this study is on the effects of the insoluble surfactant on interfacial dynamics of thin liquid films and elasticity number is, therefore, one important parameter to be considered since the surfactant is assumed to be uniformly distributed at the interface. The elasticity number, β, which characterizes the response of interfacial tension to changes in surfactant concentration is given as

$$\beta = \frac{MC_0}{\Sigma_0} = \frac{Wi}{Re}, \tag{25}$$

here, Σ_0, is the interfacial tension of the interface without surfactants, Wi is Weissenberg number and Re is Reynolds number.

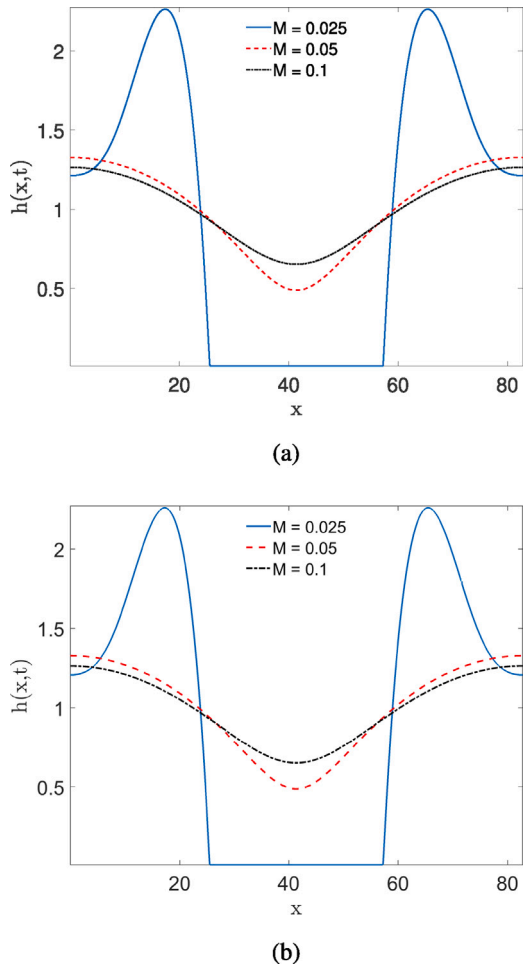

Fig. 10. Evolution of three thin films for $b = 1$, $\lambda_2 = 0.01$, $M = 0.025$ (blue solid lines), 0.05 (red dashed lines), 0.1(black dotted lines) at early time regime, $t = 8.16 \times 10^4$, when (a) $\lambda_1 = 4$ and (b) $\lambda_1 = 10$.

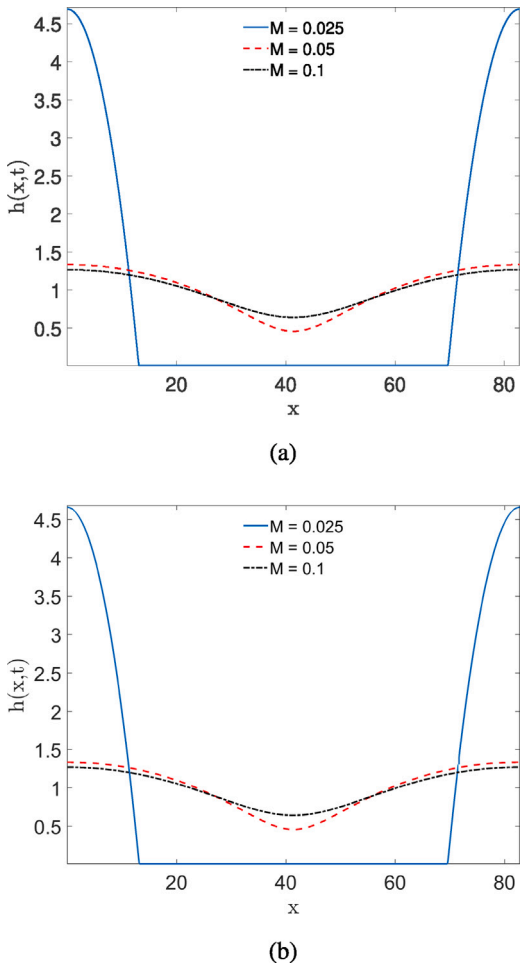

Fig. 11. Evolution of three thin films for $b = 1$, $\lambda_2 = 0.01$, $M = 0.025$ (blue solid lines), 0.05 (red dashed lines), 0.1(black dotted lines) at middle time regime, $t = 8.2 \times 10^4$, when (a) $\lambda_1 = 4$ and (b) $\lambda_1 = 10$.

The elasticity number can be related to the interfacial tension corresponding to the initial uniformly distributed surfactant with concentration, C_0, as

$$\Sigma = \Sigma_0(1 - \beta), \tag{26}$$

Therefore, the effects of the surfactant on thin film interfacial dynamics by varying β is studied. Fig. 14 shows the thin film responses to varying values of elasticity number at three different time regimes $t = 3.45 \times 10^5$ (Fig. 14(a)), 3.56×10^5 (Fig. 14(b)) and 4.0×10^5 (Fig. 14(c)) respectively. Here, a linear relationship between interfacial tension and surfactant concentration is considered. Three values of elasticity number are tested while letting flow patterns dominate the elastic and the viscous forces. The thin film evolutions follow similar trend that is observed for changes in the Marangoni number. Dewetting of the substrate reduces with increasing elasticity number. The linear relationship (Eq. (25)) fails when the Weissenberg number is equal or greater than the Reynolds number.

Beside the surfactant concentration gradient and elasticity number, the Marangoni stress can also be determined by the dependence of interfacial tension on local surfactant concentration. Although the linear equation of state is used in the present study, the relation is often nonlinear in practice, especially at high surface coverage of the surfactant [40]. Thus, it is necessary to examine the Marangoni effect on the dynamics of viscoelastic thin liquid films when a nonlinear equation of state is employed for the relation. The following typical example of the nonlinear equation of state, Eq. (24), derived from Langmuir adsorption is used [41].

$$\Sigma = 1 + \beta ln(1 - x_{CO}C), \tag{27}$$

where $x_{CO} = C_0/C_\infty$ is the dimensionless surfactant coverage, which is set to 0.1 in this study.

The thin film evolutions and responses to changes in elasticity number when there is nonlinear relationship between interfacial tension and surfactant concentration are shown in Fig. 15. Nonlinearity leads to higher film growth and rupturing compared to results for the linear relationship reported in Fig. 14. The response of the films to variations in the values of the elasticity number is similar to the observations for linear relationships. The faster separation of the rims as shown in Fig. 15(a) through Fig. 15(c) indicates how long the substrate stays exposed. For $\beta = 0.1$, the number of secondary droplets reduces from 25 at $t = 3.45 \times 10^5$ (Fig. 15(a)) to 16 at $t = 3.56 \times 10^5$ (Fig. 15(b)) and 10 at 4.0×10^5 (Fig. 15(c)). The number of secondary droplets increases with an increased elasticity number such that for $\beta = 0.2$, the number of secondary droplets reduces from 39 at $t = 3.45 \times 10^5$ (Fig. 15(a)) to 19 at $t = 3.56 \times 10^5$ (Fig. 15(b)) but also 10 at 4.0×10^5 (Fig. 15(c)). The film with $\beta = 0.3$ shows slow dynamics (Fig. 15(a)) but ruptured into 23 secondary droplets at $t = 3.56 \times 10^5$ (Fig. 15(b)) and reduced to 8 droplets at 4.0×10^5 (Fig. 15(c)).

Fig. 16 shows the evolution of four distinct films at late time regime when the product of the Marangoni number and the surfactant concentration (MC_0) or the Weissenberg number is equal to or greater than

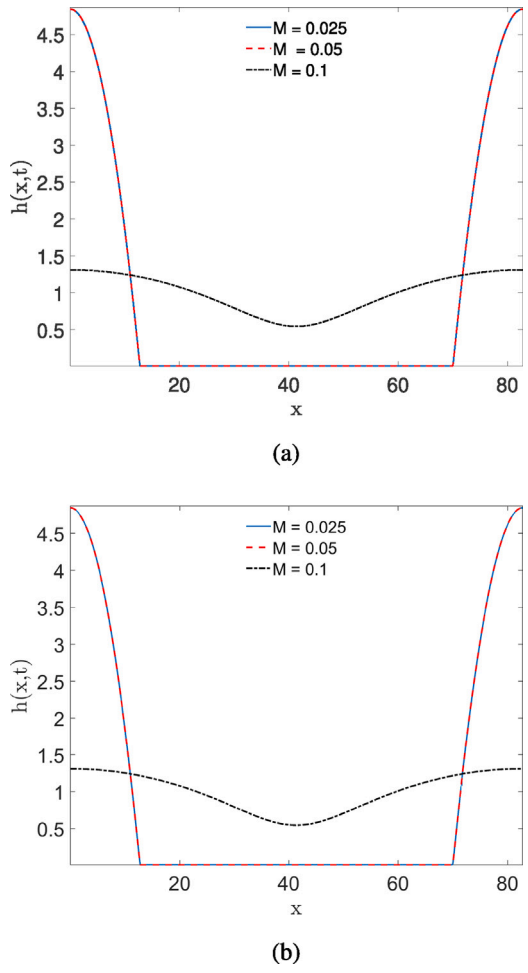

Fig. 12. Evolution of three thin films for $b = 1$, $\lambda_2 = 0.01$, $M = 0.025$ (blue solid lines), 0.05 (red dashed lines), 0.1(black dotted lines) at late time regime, $t = 8.5 \times 10^4$, when (a) $\lambda_1 = 4$ and (b) $\lambda_1 = 10$.

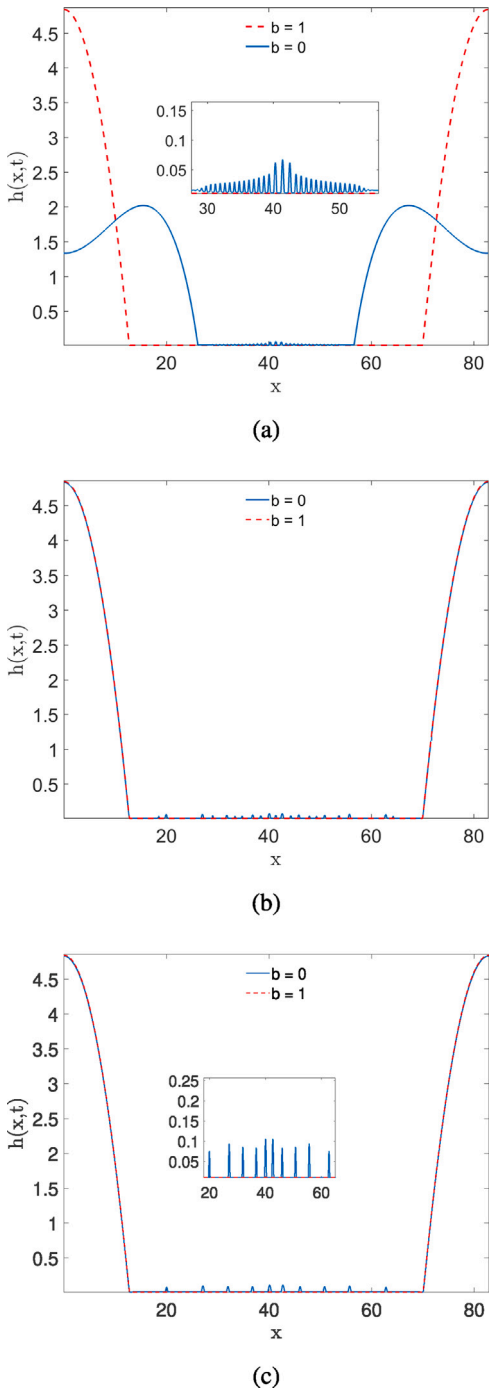

Fig. 13. Evolution of three thin films for $\lambda_1 = 10$, $\lambda_2 = 0.01$, $M = 0.025$, $b = 0$ (blue solid lines), 1 (red dashed lines) at (a) early time regime, $t = 3.45 \times 10^5$, (b) middle time regime, $t = 3.56 \times 10^5$ and (c) late time regime, $t = 4.0 \times 10^5$. The insert is a closed in on the secondary droplets formed when no slip boundary condition is applied.

the constant part of the interfacial tension (Σ_0) or the Reynold number for nonlinear relationship between interfacial tension and surfactant concentration i.e., for $\beta > 1$. Film growth and rupturing correspond to variations in elasticity number and exposure time. However, the effects of the Marangoni number becomes less pronounced compared to the observed film evolutions when the dimensionless interfacial tension for the constant part of the interfacial tension, (Σ_0) is greater than the product of the Marangoni number and surfactant concentration. Meanwhile, a higher elasticity number reduces the speed at which the secondary droplets are formed.

5. Analysis of the shape in the dewetted region

Rauscher et al. [24] performed a linear stability analysis to investigate the shape of the rim of a dewetting viscoelastic thin film. The authors concluded that the analysis would result in two negative real parts of the growth rate and concluded that normal modes with negative real ω cannot be a solution to the equation for the growth rate. Similarly, Barra et al. [1] observed that the linearized solution in the dewetted region, under quasi steady state conditions, does not depend on the viscoelastic parameters. Hence, they found that "the oscillations that the viscoelastic interface exhibits in the inner region of the dewetting hole cannot be analytically described with a linear analysis". In this section, we examine the contributions of the dimensionless interfacial tension to the linear problem of the decay of the capillary response the opening hole creates towards the flat film state.

To study the correlations between the number of droplets and the wavenumber of the most unstable mode, we analyse the observed oscillations in the dewetted region according to the linear analysis presented in [24]. Linear stability analysis of Eqs. (17) with Q (Eq. (18))

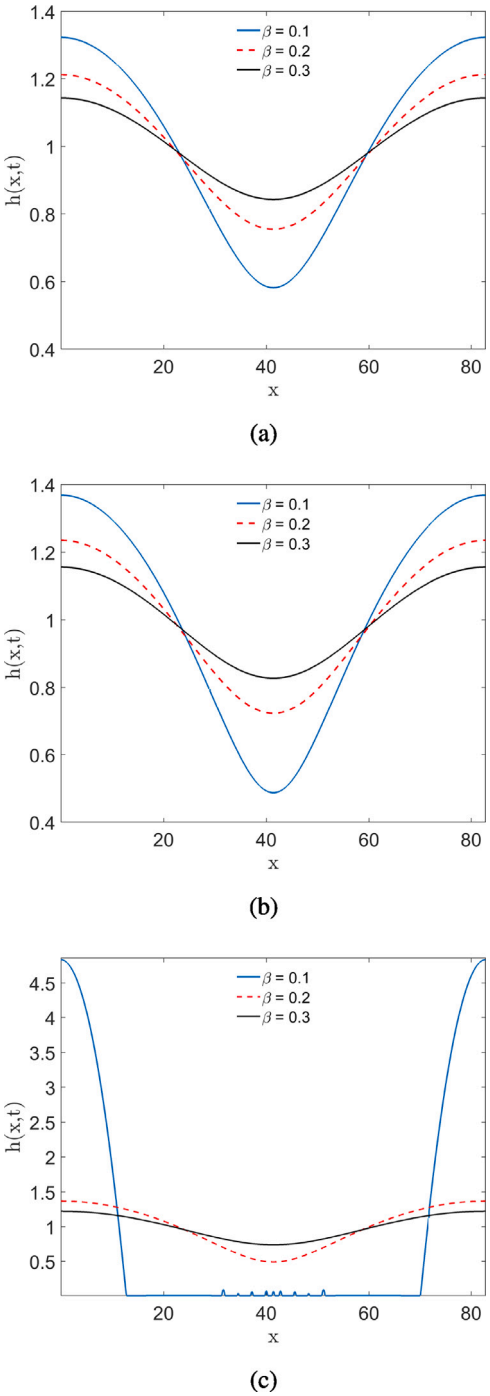

Fig. 14. Linear Evolution of three thin films for $\beta = 0.1$ (blue solid lines), 0.2 (red dashed lines), 0.3 (black straight lines) at (a) early time regime, $t = 3.45 \times 10^5$, (b) middle time regime, $t = 3.56 \times 10^5$ and (c) late time regime, $t = 4.0 \times 10^5$.

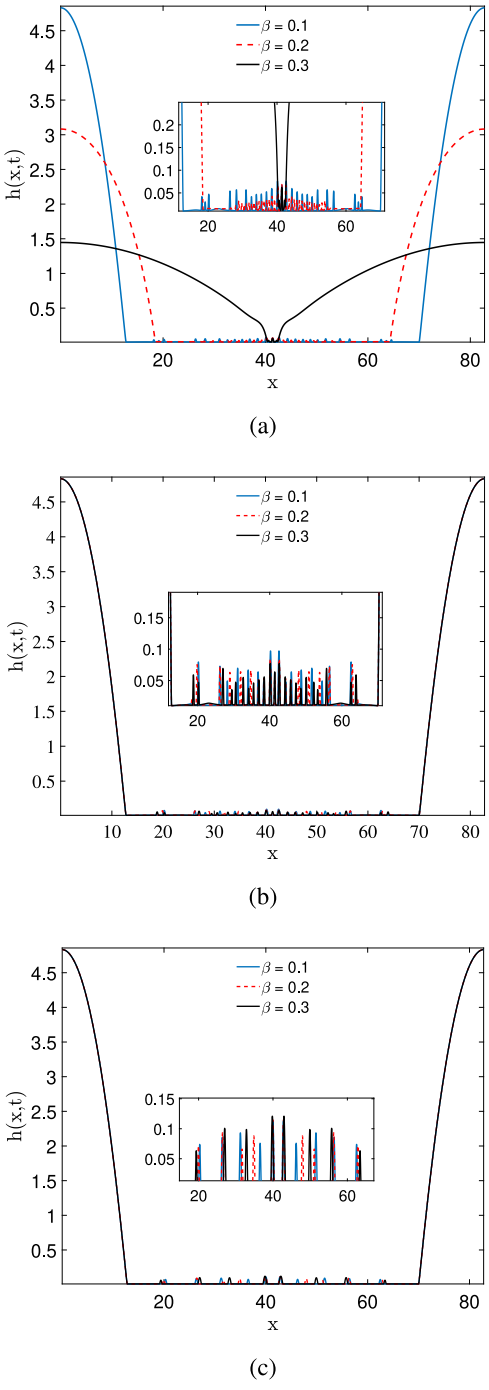

Fig. 15. Evolution of three thin films for nonlinear relationship between interfacial tension and surfactant concentration at $\beta = 0.1$ (blue solid lines), 0.2 (red dashed lines), 0.3 (black straight lines) at (a) early time regime, $t = 3.45 \times 10^5$, (b) middle time regime, $t = 3.56 \times 10^5$ and (c) late time regime, $t = 4.0 \times 10^5$.

and R (Eq. (19)) are conducted for the 2-dimensional situation of a cross-section of the growing hole. The van der Waals force contribution is considered negligible since the behaviour near the contact line is not of interest in this analysis.

If the co-ordinate system is shifted to the frame co-moving with the growing hole located at s(t), i.e.

$$h(x,t) = h(\xi,t), \quad Q(x,t) = Q(\xi,t), \quad R(x,t) = R(\xi,t) \quad \text{with} \quad \xi = x - s(t), \tag{28}$$

where Q and R are the first components of Eqs. (18) and (19) in two dimensions, we have

$$\begin{aligned} &\frac{\partial h}{\partial t} - \dot{s}\frac{\partial \xi}{\partial h} + \lambda_2 \left(\frac{\partial^2 h}{\partial t^2} - 2\dot{s}\frac{\partial}{\partial t}\left(\frac{\partial h}{\partial \xi}\right) + \dot{s}^2 \frac{\partial^2 h}{\partial \xi^2} - \ddot{s}\frac{\partial h}{\partial \xi} \right) \\ &\quad + (\lambda_2 - \lambda_1)\frac{\partial}{\partial \xi}\left[\left(\frac{\partial h}{\partial t} - \dot{s}\frac{\partial h}{\partial \xi} \right) \left(\frac{h^2}{2} Q - hR \right) \right] \\ &= \frac{\partial}{\partial \xi}\left[-\left(\frac{h^3}{3} + bh^2 \right) \Sigma \frac{\partial^3 h}{\partial \xi^3} - \frac{\partial}{\partial t}\left\{ \left(\lambda_1 \frac{h^3}{3} + \lambda_2 bh^2 \right) \Sigma \frac{\partial^3 h}{\partial \xi^3} \right\} \right. \\ &\quad \left. + \dot{s}\frac{\partial}{\partial \xi}\left\{ \left(\lambda_1 \frac{h^3}{3} + \lambda_2 bh^2 \right) \Sigma \frac{\partial^3 h}{\partial \xi^3} \right\} \right], \end{aligned} \tag{29}$$

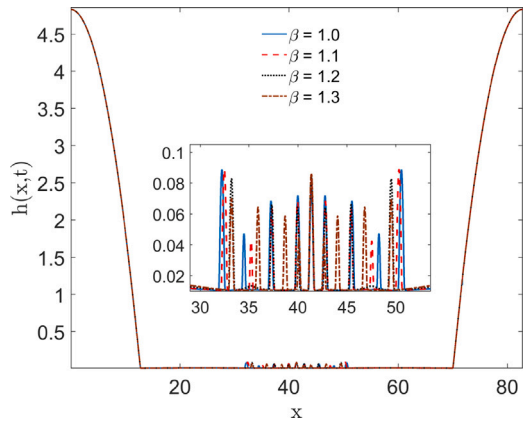

Fig. 16. Nonlinear Evolution of three thin films for $\beta = 1.0$ (blue solid lines), 1.1 (red dashed lines), 1.2 (black straight lines) and 1.3 (brown dash lines) at the late time regime, $t = 4.0 \times 10^5$.

together with

$$\left(1 + \lambda_2 \frac{\partial}{\partial t} - \lambda_2 \dot{s} \frac{\partial}{\partial \xi}\right) Q = -\Sigma \frac{\partial^3 h}{\partial \xi^3}, \tag{30}$$

$$\left(1 + \lambda_2 \frac{\partial}{\partial t} - \lambda_2 \dot{s} \frac{\partial}{\partial \xi}\right) R = -h\Sigma \frac{\partial^3 h}{\partial \xi^3}. \tag{31}$$

If a quasi-steady state is assumed in which the shape of the rim in the dewetted region changes only slowly and the speed $\dot{s}$ is constant, a linearized form of the perturbation Eqs. (29)–(31) is obtained (see Rauscher et al. [24]. Solving the linearized equation would always have a growth rate ω with a negative real part in the following equation for the growth rate,

$$\begin{aligned} &-\dot{s} + \lambda_2 \dot{s}^2 \omega + \left(\frac{h_0^3}{3} + b h_0^2\right) \Sigma \omega^3 \\ &-\dot{s}\left(\lambda_1 \frac{h_0^3}{3} + \lambda_2 b h_0^2\right) \Sigma \omega^4 = 0. \end{aligned} \tag{32}$$

The influence of dimensionless interfacial tension, Σ, and therefore, the Marangoni number is significant and can serve as either increasing or reducing factor in the coefficients of both the third and fourth order in ω. It can be concluded from Eq. (32) that the oscillations exhibited by viscoelastic thin films can only be described analytically if the product of Marangoni number and surfactant concentration is large enough to exceed the value of the constant part of the dimensionless interfacial tension.

6. Conclusion

A modified nonlinear evolution equation for viscoelastic thin films bounded below by a solid substrate and above by liquid–liquid interface is presented. The effects of gradient of interfacial tension is considered on the responses of the thin films to prescribed perturbation. Model formulation reveals that both the capillary and van der Waals components of the pressure term are affected by the properties of the thin film including the fluid–fluid interactions. Linear stability analysis shows that the region of stability of the films is affected by the Marangoni number, tension, slip length and contact angle.

We verified the following observations: (1). The dynamics of the thin films varies greatly across different time regimes. Most of the actions occurred at early time regime when the films developed and at the late time regime when the rims tend to separate. (2). Increase in the characteristic relaxation time leads to the formation of multiple secondary droplets and stability in the film behaviour, respectively.

Integration of the Marangoni number into thin film evolution equation allows the study of how interfacial dynamics is influenced by interfacial tension gradients. High variations in interfacial tension gradient reduces growth rate and rupturing of thin films in the presence of surfactants. A linear relationship between interfacial tension and surfactant concentration can only be assumed where the product of the Marangoni number and surfactant concentration does not exceed the dimensionless interfacial tension for the constant part of the interfacial tension. Otherwise, a nonlinear correlation between dimensionless interfacial tension and surfactant concentration is required to describe viscoelastic flow at interfaces. The application of a nonlinear relationship between interfacial tension and surfactant concentration leads to faster film dynamics and rupturing speed.

Declaration of competing interest

The authors declare that they have no known competing financial interests or personal relationships that could have appeared to influence the work reported in this paper.

Data availability

No data was used for the research described in the article.

Acknowledgements

The authors Bamikole Adeyemi, Prashant Jadhawar, and Lateef Akanji wish to appreciate the support of Petroleum Technology Development Fund (PTDF), Nigeria for this project.

Appendix. Derivation of the long wave approximation

The two mutually orthogonal vectors **n** and **t** are defined as

$$\mathbf{n} = \frac{\left(\frac{-\partial h}{\partial x}, 1\right)}{\left[1 + \left(\frac{\partial h}{\partial x}\right)^2\right]^{\frac{1}{2}}} \tag{33}$$

$$\mathbf{t} = \frac{\left(1, \frac{\partial h}{\partial x}\right)}{\left[1 + \left(\frac{\partial h}{\partial x}\right)^2\right]^{\frac{1}{2}}} \tag{34}$$

and

$$\kappa = -\nabla \cdot \mathbf{n} = \frac{\left(\frac{\partial^2 h}{\partial x^2}, 1\right)}{\left[1 + \left(\frac{\partial h}{\partial x}\right)^2\right]^{\frac{3}{2}}}. \tag{35}$$

Other parameters can be further scaled as follows

$$X = \frac{x}{L}, \tag{36}$$

$$(Y, H, B) = \frac{1}{h_0}(y, h, b). \tag{37}$$

If the characteristic velocity of the problem is denoted by u_0, then

$$U = \frac{u}{u_0}, V = \frac{v}{(\epsilon u_0)}, \tag{38}$$

$$(t^*, \lambda_1^*, \lambda_2^*) = \frac{1}{T}(t, \lambda_1, \lambda_2), \tag{39}$$

$$\tau_{ij}{}^* = \frac{T}{\mu}\tau_{ij}, \tag{40}$$

$$p_o = \frac{\mu}{(T\epsilon^2)}, \tag{41}$$

$$T = \frac{L}{u_0}, \tag{42}$$

$$Re = \frac{(\rho u_0 L)}{\mu}. \tag{43}$$

All quantities are, therefore, considered from now on dimensionless but original notations will be maintained to avoid cumbersomeness.

Substituting the scaled forms into Eq. (1), the following system is obtained:

$$\epsilon Re\frac{\partial u}{\partial t} = \epsilon^2\frac{\partial \tau_{11}}{\partial x} + \frac{\partial \tau_{21}}{\partial y} - \frac{\partial p}{\partial x}, \tag{44}$$

$$\epsilon^3 Re\frac{\partial u}{\partial t} = \epsilon^2\left(\frac{\partial \tau_{12}}{\partial x} + \frac{\partial \tau_{22}}{\partial y}\right) - \frac{\partial p}{\partial y}. \tag{45}$$

The dimensionless components of the stress tensor given by the Jeffreys model, Eq. (6), satisfy

$$\tau_{11} + \lambda_1\frac{\partial \tau_{11}}{\partial t} = 2\left(\frac{\partial u}{\partial x} + \lambda_2\frac{\partial}{\partial t}\left(\frac{\partial u}{\partial x}\right)\right), \tag{46}$$

$$\tau_{22} + \lambda_1\frac{\partial \tau_{22}}{\partial t} = 2\left(\frac{\partial v}{\partial y} + \lambda_2\frac{\partial}{\partial t}\left(\frac{\partial v}{\partial y}\right)\right), \tag{47}$$

$$\begin{aligned}\tau_{12} + \lambda_1\frac{\partial \tau_{12}}{\partial t} &= \frac{\partial u}{\partial y} + \lambda_2\frac{\partial}{\partial t}\left(\frac{\partial u}{\partial y}\right)\\ &+\epsilon^2\left(\frac{\partial v}{\partial x} + \lambda_2\frac{\partial}{\partial t}\left(\frac{\partial v}{\partial x}\right)\right).\end{aligned} \tag{48}$$

The leading-order terms in the governing Eqs. (44) and (45) respectively, are

$$\frac{\tau_{21}}{\partial y} = \frac{\partial p}{\partial x}, \tag{49}$$

$$\frac{\partial p}{\partial y} = 0. \tag{50}$$

Integrating Eq. (49), we have

$$\tau_{21} = \frac{\partial p}{\partial x}(y-h). \tag{51}$$

Substituting τ_{21} into Eq. (48), we obtain (up to the leading order)

$$\frac{\partial p}{\partial x}(y-h) + \lambda_1\frac{\partial}{\partial t}\left(\frac{\partial p}{\partial x}(y-h)\right) = \frac{\partial u}{\partial y} + \lambda_2\frac{\partial}{\partial t}\left(\frac{\partial u}{\partial y}\right), \tag{52}$$

$$\left(1+\lambda_2\frac{\partial}{\partial t}\right)\left(\frac{\partial u}{\partial y}\right) = \left(1+\lambda_1\frac{\partial}{\partial t}\right)(y-h)\frac{\partial p}{\partial x}. \tag{53}$$

Integrating Eq. (53) from $y = 0$ to $y = h(x,t)$ using the corresponding boundary conditions, we have

$$\left(1+\lambda_2\frac{\partial}{\partial t}\right)[u]_0^{h(x,t)} = \left(1+\lambda_1\frac{\partial}{\partial t}\right)\left(\frac{1}{2}y^2 - hy\right)\frac{\partial p}{\partial x}. \tag{54}$$

Applying the boundary conditions we obtain

$$\left(1+\lambda_2\frac{\partial}{\partial t}\right)\left[u + bh\frac{\partial p}{\partial x}\right] = \left(1+\lambda_1\frac{\partial}{\partial t}\right)\left(\frac{1}{2}y^2 - hy\right)\frac{\partial p}{\partial x}, \tag{55}$$

$$\left(1+\lambda_2\frac{\partial}{\partial t}\right)u + \left(1+\lambda_2\frac{\partial}{\partial t}\right)bh\frac{\partial p}{\partial x} = \left(1+\lambda_1\frac{\partial}{\partial t}\right)\left(\frac{1}{2}y^2 - hy\right)\frac{\partial p}{\partial x}, \tag{56}$$

$$u + \lambda_2\frac{\partial}{\partial t}u = m, \tag{57}$$

with

$$m = \left(1+\lambda_1\frac{\partial}{\partial t}\right)\left(\frac{1}{2}y^2 - hy\right)\frac{\partial p}{\partial x} - \left(1+\lambda_2\frac{\partial}{\partial t}\right)bh\frac{\partial p}{\partial x}. \tag{58}$$

The solution to Eq. (56) can be represented as

$$u = \frac{1}{\lambda_2}\int_{-\infty}^{t} e^{-\frac{t-t'}{\lambda_2}} m(x,y,t')dt'. \tag{59}$$

Integrating Eq. (56) from 0 to $y = h(x,t)$ and

$$\begin{aligned}\left(1+\lambda_2\frac{\partial}{\partial t}\right)\int_0^{h(x,t)} u\,dy + \left(1+\lambda_2\frac{\partial}{\partial t}\right)\int_0^{h(x,t)} bh\frac{\partial p}{\partial x}dy\\ = \int_0^{h(x,t)}\left(1+\lambda_1\frac{\partial}{\partial t}\right)\left(\frac{1}{2}y^2 - hy\right)\frac{\partial p}{\partial x}dy,\end{aligned} \tag{60}$$

$$\begin{aligned}\int_0^{h(x,t)} u\,dy + \lambda_2\frac{\partial}{\partial t}\int_0^{h(x,t)} u\,dy + bh^2\frac{\partial p}{\partial x} + \lambda_2 b\frac{\partial h^2}{\partial t}\frac{\partial p}{\partial x}\\ -\lambda_2\frac{\partial h}{\partial t}u(y=h(x,t)) - \lambda_2\frac{\partial h}{\partial t}bh\frac{\partial p}{\partial x}\\ = -\frac{h^3}{3}\frac{\partial p}{\partial x} - \lambda_1 h^2\frac{\partial h}{\partial t}\frac{\partial p}{\partial x} + \lambda_1\frac{h^2}{2}\frac{\partial h}{\partial t}\frac{\partial p}{\partial x}.\end{aligned} \tag{61}$$

Integrating the kinematic boundary condition, Eq. (4), from 0 to $y = h(x,t)$ using integration by parts gives

$$\frac{\partial h}{\partial t} + \frac{\partial}{\partial x}\left(\int_0^{h(x,t)} u\,dy\right) = 0. \tag{62}$$

Taking partial derivative of Eq. (61) and substitute it into the kinematic boundary condition Eq. (62), the long wave approximation is

$$\begin{aligned}\left(1+\lambda_2\frac{\partial}{\partial t}\right)\frac{\partial h}{\partial t} + \lambda_2\frac{\partial}{\partial x}\left[\frac{\partial h}{\partial t}u(y=h(x,t))\right]\\ = \frac{\partial}{\partial x}\left[\left(1+\lambda_1\frac{\partial}{\partial t}\right)\left(\frac{h^3}{3}\frac{\partial p}{\partial x}\right) + \left(1+\lambda_2\frac{\partial}{\partial t}\right)\left(bh^2\frac{\partial p}{\partial x}\right)\right]\\ -\frac{\partial}{\partial x}\left[\left(\lambda_1\frac{h^2}{2} + \lambda_2 bh\right)\frac{\partial h}{\partial t}\frac{\partial p}{\partial x}\right].\end{aligned} \tag{63}$$

Eq. (63) can be simplified by performing integration by parts

$$\lambda_2 u = (\lambda_2 - \lambda_1)\left(\frac{1}{2}h^2 Q - hR\right) - \left(\lambda_1\frac{1}{2}h^2 + \lambda_2 bh\right)\frac{\partial p}{\partial x}, \tag{64}$$

where, for compactness, we have used Q and R such that

$$\left(1+\lambda_2\frac{\partial}{\partial t}\right)Q = -\frac{\partial}{\partial x}\left(\frac{\partial p}{\partial x}\right), \tag{65}$$

$$\left(1+\lambda_2\frac{\partial}{\partial t}\right)R = -h\frac{\partial}{\partial x}\left(\frac{\partial p}{\partial x}\right). \tag{66}$$

Substituting for Eq. (64) in Eq. (63), the final modified form of the nonlinear evolution equation for bounded viscoelastic thin films with gradient of surfactant concentration is

$$\begin{aligned}\left(1+\lambda_2\frac{\partial}{\partial t}\right)\frac{\partial h}{\partial t}\\ +\frac{\partial}{\partial x}\left\{(\lambda_2-\lambda_1)\left(\frac{h^2}{2}Q - hR\right)\frac{\partial h}{\partial t} + \left[\left(1+\lambda_1\frac{\partial}{\partial t}\right)\frac{h^3}{3}\right.\right.\\ \left.\left.+\left(1+\lambda_2\frac{\partial}{\partial t}\right)bh^2\right]\frac{\partial}{\partial x}\left(\Sigma\frac{\partial^2 h}{\partial x^2} + w(h)\right)\right\} = 0.\end{aligned} \tag{67}$$

References

[1] V. Barra, S. Afkhami, L. Kondic, Interfacial dynamics of thin viscoelastic films and drops, J. Non-Newton. Fluid Mech. 237 (2016) 26–38, http://dx.doi.org/10.1016/j.jnnfm.2016.10.001, ID: 271393.

[2] T. Erneux, S.H. Davis, Nonlinear rupture of free films, Phys. Fluids A 5 (5) (1993) 1117–1122, http://dx.doi.org/10.1063/1.858597, 11.

[3] P.F. Green, V. Ganesan, Dewetting of polymeric films: unresolved issues, Eur. Phys. J. E 12 (3) (2003) 449–454, http://dx.doi.org/10.1140/epje/e2004-00015-6, ID: Green2003.

[4] R.J. Gumerman, G.M. Homsy, The stability of radially bounded thin films, Chem. Eng. Commun. 2 (1) (1975) 27–36, http://dx.doi.org/10.1080/00986447508960444.

[5] O.K. Matar, S.M. Troian, Linear stability analysis of an insoluble surfactant monolayer spreading on a thin liquid film, Phys. Fluids 9 (12) (1997) 3645–3657, http://dx.doi.org/10.1063/1.869502, 21.

[6] A.B. Pandit, J.F. Davidson, Hydrodynamics of the rupture of thin liquid films, J. Fluid Mech. 212 (1990) 11–24, http://dx.doi.org/10.1017/S0022112090001823.

[7] A. Oron, S.H. Davis, S.G. Bankoff, Long-scale evolution of thin liquid films, Rev. Modern Phys. 69 (3) (1997) 931–980, http://dx.doi.org/10.1103/RevModPhys.69.931, URL https://link.aps.org/doi/10.1103/RevModPhys.69.931.

[8] G.G. Fuller, J. Vermant, Complex fluid-fluid interfaces: Rheology and structure, Annu. Rev. Chem. Biomol. Eng. 3 (1) (2012) 519–543, http://dx.doi.org/10.1146/annurev-chembioeng-061010-114202, 04.

[9] K. Mahady, S. Afkhami, L. Kondic, A volume of fluid method for simulating fluid/fluid interfaces in contact with solid boundaries, J. Comput. Phys. 294 (2015) 243–257, http://dx.doi.org/10.1016/j.jcp.2015.03.051, ID: 272570.

[10] S.S. Tabakova, K.D. Danov, Effect of disjoining pressure on the drainage and relaxation dynamics of liquid films with mobile interfaces, J. Colloid Interface Sci. 336 (1) (2009) 273–284, http://dx.doi.org/10.1016/j.jcis.2009.03.084, ID: 272564.

[11] G.J. Hirasaki, Wettability: Fundamentals and surface forces, SPE Formation Evaluation 6 (02) (1991) 217–226, http://dx.doi.org/10.2118/17367-PA, J2: SPE-17367-PA.

[12] C. Maldarelli, R.K. Jain, I.B. Ivanov, E. Ruckenstein, Stability of symmetric and unsymmetric thin liquid films to short and long wavelength perturbations, J. Colloid Interface Sci. 78 (1) (1980) 118–143, http://dx.doi.org/10.1016/0021-9797(80)90501-9, ID: 272564.

[13] A.D. Wit, D. Gallez, C.I. Christov, Nonlinear evolution equations for thin liquid films with insoluble surfactants, Phys. Fluids 6 (10) (1994) 3256–3266, http://dx.doi.org/10.1063/1.868058, 30.
[14] D. Gallez, A.D. Wit, M. Kaufman, Dynamics of a thin liquid film with a surface chemical reaction, J. Colloid Interface Sci. 180 (2) (1996) 524–536, http://dx.doi.org/10.1006/jcis.1996.0333, ID: 272564.
[15] E. Ruckenstein, R.K. Jain, Spontaneous rupture of thin liquid films, J. Chem. Soc., Faraday Trans. 2: Mol. Chem. Phys. 70 (1974) 132–147, http://dx.doi.org/10.1039/F29747000132.
[16] N.M. Kovalchuk, D. Vollhardt, Marangoni instability and spontaneous non-linear oscillations produced at liquid interfaces by surfactant transfer, Adv. Colloid Interface Sci. 120 (1) (2006) 1–31, http://dx.doi.org/10.1016/j.cis.2006.01.001, ID: 271485.
[17] D. Agble, M.A. Mendes-Tatsis, The prediction of marangoni convection in binary liquid–liquid systems with added surfactants, Int. J. Heat Mass Transfer 44 (7) (2001) 1439–1449, http://dx.doi.org/10.1016/S0017-9310(00)00159-9, ID: 271451.
[18] J.R.A. Pearson, On convection cells induced by surface tension, J. Fluid Mech. 4 (5) (1958) 489–500, http://dx.doi.org/10.1017/S0022112058000616, Cited By :1344.
[19] C. Sternling, L. Scriven, Interfacial turbulence: hydrodynamic instability and the marangoni effect, AIChE J. 5 (4) (1959) 514–523.
[20] L. Steiner, G. Oezdemir, S. Hartland, Single-drop mass transfer in the water-toluene-acetone system, Ind. Eng. Chem. Res. 29 (7) (1990) 1313–1318, http://dx.doi.org/10.1021/ie00103a034.
[21] S. Slavtchev, P. Kalitzova-Kurteva, M.A. Mendes, Marangoni instability of liquid–liquid systems with a surface-active solute, Colloids Surf. A 282–283 (2006) 37–49, http://dx.doi.org/10.1016/j.colsurfa.2006.01.029, ID: 271384.
[22] S. Slavtchev, P. Kalitzova-Kurteva, M.A. Mendes, Marangoni instability of liquid–liquid systems with a surface-active solute, Colloids Surf. A 282–283 (2006) 37–49, http://dx.doi.org/10.1016/j.colsurfa.2006.01.029, ID: 271384.
[23] M. van den Tempel, E.H. Lucassen-Reynders, Relaxation processes at fluid interfaces, Adv. Colloid Interface Sci. 18 (3) (1983) 281–301, http://dx.doi.org/10.1016/0001-8686(83)87004-3, ID: 271485.
[24] M. Rauscher, A. Munch, B. Wagner, R. Blossey, A thin-film equation for viscoelastic liquids of Jeffreys type, Eur. Phys. J. E 17 (3) (2005) 373–379, http://dx.doi.org/10.1140/epje/i2005-10016-8, ID: Rauscher2005.
[25] V. Barra, S. Afkhami, L. Kondic, Thin viscoelastic dewetting films of jeffreys type subjected to gravity and substrate interactions, Eur. Phys. J. E 42 (1) (2019) 12, http://dx.doi.org/10.1140/epje/i2019-11774-2, ID: Barra2019.
[26] Q.-f. Fu, T. Hu, L.-j. Yang, Instability of a weakly viscoelastic film flowing down a heated inclined plane, Phys. Fluids 30 (8) (2018) 084102, http://dx.doi.org/10.1063/1.5041494, 02.
[27] R. Sarma, P.K. Mondal, Thermosolutal Marangoni instability in a viscoelastic liquid film: effect of heating from the free surface, J. Fluid Mech. 909 (2021) A12, http://dx.doi.org/10.1017/jfm.2020.880.
[28] R.B. Bird, R.C. Armstrong, O. Hassager, Dynamics of Polymeric Liquids Vol 1, 2nd Ed: Fluid Mechanics, John Wiley and Sons Inc, United States, 1987, URL http://inis.iaea.org/search/search.aspx?orig_q=RN:18088690.
[29] G. Tomar, V. Shankar, S.K. Shukla, A. Sharma, G. Biswas, Instability and dynamics of thin viscoelastic liquid films, Eur. Phys. J. E 20 (2) (2006) 185–200, http://dx.doi.org/10.1140/epje/i2006-10011-7, ID: Tomar2006.
[30] G.F. Teletzke, T.D. H., L.E. Sciven, How liquids spread on solids, Chem. Eng. Commun. 55 (1–6) (1987) 41–82, http://dx.doi.org/10.1080/00986448708911919.
[31] J.A. Diez, L. Kondic, On the breakup of fluid films of finite and infinite extent, Phys. Fluids 19 (7) (2007) 072107, http://dx.doi.org/10.1063/1.2749515, arXiv:http://dx.doi.org/10.1063/1.2749515.
[32] I. Seric, S. Afkhami, L. Kondic, Interfacial instability of thin ferrofluid films under a magnetic field, J. Fluid Mech. 755 (2014) R1, http://dx.doi.org/10.1017/jfm.2014.435.
[33] V. Alvarado, M.M. Bidhendi, G. Garcia-Olvera, B. Morin, J.S. Oakey, Interfacial visco-elasticity of crude oil - brine: An alternative EOR mechanism in smart waterflooding, 2014, http://dx.doi.org/10.2118/169127-MS, SPE–169127–MS.
[34] H. Ding, S. Rahman, Experimental and theoretical study of wettability alteration during low salinity water flooding-an state of the art review, Colloids Surf. A 520 (2017) 622–639, http://dx.doi.org/10.1016/j.colsurfa.2017.02.006, ID: 271384.
[35] K. Takamura, R.S. Chow, A mechanism for initiation of bitumen displacement from oil sand, J. Can. Pet. Technol. 22 (06) (1983) http://dx.doi.org/10.2118/83-06-01.
[36] F. Mugele, B. Bera, A. Cavalli, I. Siretanu, A. Maestro, M. Duits, M. Cohen-Stuart, D. van den Ende, I. Stocker, I. Collins, Ion adsorption-induced wetting transition in oil-water-mineral systems, Sci. Rep. 5 (1) (2015) 10519, http://dx.doi.org/10.1038/srep10519, ID: Mugele2015.
[37] R.D. Tewari, A.Y. Dandekar, J.M. Ortiz, Petroleum Fluid Phase Behavior: Characterization, Processes, and Applications, CRC Press, 2018, URL https://books.google.co.uk/books?id=nIuADwAAQBAJ.
[38] V. Barra, valeriabarra/ThinViscoelasticFilms: v0.1, Zenodo, 2019, http://dx.doi.org/10.5281/zenodo.3561225.
[39] L. Kondic, Instabilities in gravity driven flow of thin fluid films, SIAM Rev. 45 (1) (2003) 95–115, http://dx.doi.org/10.1137/S003614450240135, 12.
[40] R.A. Johnson, A. Borhan, Effect of insoluble surfactants on the pressure-driven motion of a drop in a tube in the limit of high surface coverage, J. Colloid Interface Sci. 218 (1) (1999) 184–200, http://dx.doi.org/10.1006/jcis.1999.6376, ID: 272564.
[41] M. Muradoglu, G. Tryggvason, Simulations of soluble surfactants in 3D multiphase flow, J. Comput. Phys. 274 (2014) 737–757, http://dx.doi.org/10.1016/j.jcp.2014.06.024, ID: 272570.